TURBULENCE CONTROL OF AERONAUTICAL FLOWS WITH PLASMA-INDUCED JETS

14th International Symposium on Turbulence and Shear Flow Phenomena (TSFP14)
Heidelberg, Germany, July 28–31, 2026

TURBULENCE CONTROL OF AERONAUTICAL FLOWS WITH PLASMA-INDUCED JETS

J. Serpieri*, **E. Fracchia, G. Cafiero,**
Department of Mechanical and Aerospace Engineering, Politecnico di Torino
Turin, 10129, Italy
* jacopo.serpieri@polito.it

L. Magnani, A. Talamelli, G. Bellani,
Department of Industrial Engineering
University of Bologna
Forlì, 47121, Italy

C. Willert
DLR Institute for Propulsion Technology
German Aerospace Center
Köln, 50931, Germany

ABSTRACT

In this study, we present a first attempt to control wall turbulence at high friction Reynolds numbers ($Re_\tau \approx 8\,000\,\&\,14\,400$) by means of an array of sinusoidally-shaped, wall-mounted plasma actuators. While the final aim is to reduce friction drag by disrupting the wall turbulence cycle, this study presents a preliminary effort in assessing whether the deployed flow control approach is effective in controlling turbulence at high Reynolds numbers. The experiments were carried out in the world-unique Long Pipe facility at the CICLoPE laboratory. High-speed, high-resolution particle image velocimetry captured the effects of the performed flow control. The presented results show the potential of these actuators of having a significant impact on the turbulent statistics and on the spectral signature of the turbulent fluctuations at both the tested flow velocities. Specifically, while the streamwise velocity fluctuations near the wall are reduced, those in the logarithmic layer appear to be enhanced.

MOTIVATION

Turbulent skin friction accounts for more than the 50% of the total drag on an airliner in cruise flight. As such reducing friction drag is a crucial effort for a cleaner aviation.

Geometric features on the flow-wetted surfaces as the riblets interfere with the wall turbulence regeneration cycle and showed to reduce friction drag of some percentage points (e.g. Bechert & Bartenwerfer, 1989; Walsh, 2012). Besides passive flow control approaches, active ones have also emerged with the aim of increasing both the level of achievable drag reduction and their operational range – as active devices allow to tune some of their control parameters following diverse flow conditions –. Among the active flow control efforts, oscillating the wall along the cross- or span-wise direction showed to effectively disrupt the turbulence coherent structures and the effect they cause on friction drag (e.g. Jung *et al.*, 1992; Choi & Graham, 1998). Nevertheless, such a flow control approach is cumbersome to implement. Because of this, oscillating wall like forcing approaches have been explored in the literature. Arrays of wall-mounted plasma actuators (PAs), designed to induce an oscillating flow or other control flows, can also reduce friction drag while simplifying the actuator embodiment and installation (e.g. Wilkinson, 2003; Jukes *et al.*, 2006; Choi *et al.*, 2011; Whalley & Choi, 2014; Thomas *et al.*, 2019; Hehner *et al.*, 2019; Serpieri *et al.*, 2023; Fang *et al.*, 2024; Wei & Zhou, 2025). With the aim of replicating the oscillation forcing but with passive means and leveraging on the flow advection, riblets modulated sinusoidally along the streamwise direction were also proposed and showed to outperform the original longitudinal ones (e.g. Peet & Sagaut, 2009; Sasamori *et al.*, 2014, 2017; Cafiero *et al.*, 2024). Besides these efforts, wall-normal jets also proved to be capable of weakening the turbulence larger structures with beneficial effects on friction drag (e.g. Schoppa & Hussain, 1998; Iuso *et al.*, 2002).

In this study and following the work of Benard *et al.* (2024), we combined these different approaches and we developed an array of sinusoidally modulated PAs inducing wall-tangential jets in opposing directions, eventually colliding and forming wall-normal plumes. The aim of the study is to actively – and with a relatively simple, retrofitting flow actuator – control the turbulence cycle for aeronautical flows. The developed PA array was therefore designed to match the turbulence scales at high friction Reynolds numbers ($Re_\tau \approx 8\,000\,\&\,14\,400$) possible in the CICLoPE Long Pipe (LP) facility.

EXPERIMENTAL SETUP

The CICLoPE LP is a world-unique facility for studying turbulence for aeronautical flows allowing for high (friction) Reynolds number flows ($Re_\tau > 45\,000$) at still measurable scales. It consists of a 111.15 m long pipe and a diameter $D = 0.90$ m, where dynamically and thermally stable conditions can be generated (Bellani & Talamelli, 2016; Zheng *et al.*, 2022).

The pipe is equipped with several round access ports for the installation of measurement instrumentation such as hotwires, pressure probes or optical equipment. For the present investigation, we designed and 3D printed an insert for the access port to accommodate both a bay to flush mount

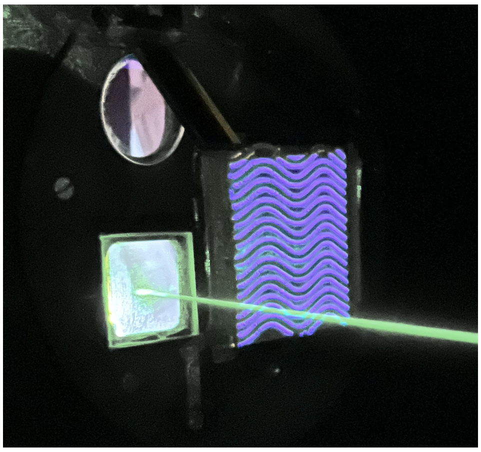

Figure 1. Photograph of the flow control and diagnostics insert, seen from inside the pipe (flow from right to left), featuring: the PA array, installed more upstream and operated (see the plasma discharges glowing in violet) and the optical windows: the upper, circular one for the camera view facing a $\approx 45°$-slanted mirror and the lower, squared one for the laser light sheet (see the light green beam).

the PA array and to allow for their electrical connections, and to install the optical elements needed to investigate the controlled flow. These were mounted 25 mm downstream of the downstream edge of the plasma discharge region (corresponding to 450 l_τ at $Re_\tau = 8\,000$ and to 830 l_τ at $Re_\tau = 14\,400$, with $l_\tau = \nu/u_\tau$ being the turbulence viscous length scale, u_τ the friction velocity and ν the kinematic viscosity) and roughly centered along the azimuthal direction. A photograph of the mentioned access port insert, equipped with the operated PA array, the optical elements and the laser beam, as seen from inside the pipe, is shown in Figure 1.

The considered array of plasma actuators had an extension along the streamwise direction of $L_x = 65$ mm with a streamwise wavelength of the sinusoidal wave of $\lambda_x = 32$ mm whereas the array extension and the electrodes spacing along the spanwise/azimuthal direction were $L_z = 60$ mm and $\lambda_z = 6$ mm (see Figure 2). These quantities are made non dimensional using l_τ for the two different Reynolds numbers and are reported in Table 1, with the canonical + superscript used for inner units scaled quantities. The peak-to-peak amplitude of the wave (a) was $a = \lambda_z$. The array featured silver-paint electrodes hair-brush deposited on the air-exposed side of a PET 0.5 mm thick dielectric substrate. To accurately paint these electrodes, a laser-cut stencil stencil was made from a black adhesive film. The exposed electrodes were fed with a high voltage signal supplied by a GBS Elektronik Minipuls 4 powered by a stabilized DC power supply and supplied with a square wave signal oscillating at a frequency of 9 kHz – as most of the dielectric barrier discharge (DBD) actuators work on AC signals –. Two different peak-to-peak voltage amplitudes (V_{pp}) were considered: 8 and 10 kV, leading to plasma jets of different strength. The induced velocity consists of two wall-parallel jets, emitted from the two sides of the exposed electrodes, eventually meeting around the centerline of the encapsulated electrodes and merging into wall-normal outboard-directed plumes. The actuator induced flow-field was analyzed from an ad hoc PIV experiment in quiescent air – not discussed here for conciseness – at the two operated voltages. The resulting maximum value of the induced wall normal velocity was $\max(V_{PA}) = 0.19$ m/s at $V_{pp} = 8\,$kV, while $\max(V_{PA}) = 0.23$ m/s for the $V_{pp} = 10\,$kV case. The minimum induced velocity value was $\min(V_{PA}) \approx -0.15$ m/s for both the supplied voltages. Also these values are made non-dimensional using the friction velocity (u_τ) for both the tested flows and are reported in Table 1. The array encapsulated electrodes were made instead with copper tape covering the whole other side of the dielectric layer and were electrically isolated with several layers of Kapton tape. These electrodes were connected to the ground terminal of the building. The array was mounted on the 3D printed pipe access insert by means of double-sided tape. Moreover, to reduce the effect of possible gaps, dips, and protrusions between the PA array and its bay, Kapton tape was placed on all the interfaces. The electrical connection of the PA electrodes was made with adhesive copper-tape strips between the electrodes and some metallic bolts embedded in the pipe insert and crossing its whole thickness such to offer electric connections on the outer shell of the pipe.

High speed planar PIV was deployed to investigate the flow control effect downstream of the PA array. The optical configuration replicated the one of Willert *et al.* (2017), as shown in Figure 1. In this case, a high-speed camera (Vision Research T4040) equipped with a tele-macro lens (Nikon Micro-Nikkor 200/4) observed a narrow wall-normal field of view (FOV) through an upper round window and a $\approx 45°$ inclined mirror. The FOV extended of 2 mm along the streamwise (x) direction and of 25 mm along the wall-normal one (y). It was illuminated with an $\approx 0.20\,$mm thin light sheet in the azimuthal direction, formed by a pair of pulsed lasers (Innolas Photonics/Iradion Nanio Air 532-10-V-SP). Image magnification was set to unity, with one camera pixel corresponding to $9.3\,\mu$m in object space which respectively corresponds to 5.9 and 3.1 pixel per viscous length.

Two different measurement types were performed. The first type, aimed at obtaining statistically converged velocimetry data, featured a lower sampling frequency ($f_s = 0.8$ kHz for the $Re_\tau = 8\,000$ case and $f_s = 1.6$ kHz for the $Re_\tau = 14\,400$ case) and consisted of $1.0 \cdot 10^5$ samples (N_s), acquired in frames straddling mode. The related large-eddy turnover times, computed as $\frac{N_s U_{cl}}{f_s D/2}$, with U_{cl} being the pipe centerline velocity measured with a Prandtl tube, are reported in Table 1. The second measurement type instead was performed at a higher sampling frequency ($f_s = 30$ kHz for the $Re_\tau = 8\,000$ case, leading to an inner-scales non dimensional sampling time of $t^+ = \frac{u_\tau^2}{\nu f_s} = 0.16$ and $f_s = 60$ kHz for the $Re_\tau = 14\,400$ case, leading to $t^+ = 0.28$) to guarantee a Nyquist frequency large enough to resolve most of the higher-frequency portion of the turbulent spectra. These measurements consisted of $1.8 \cdot 10^5$ frames, acquired in sequence.

The acquired images were first preprocessed to reduce light reflections from the wall and the slight wall wobbling caused by the vibrations of the setup or the slight deformation of the PA array caused by heating from the plasma discharge and were batch-processed with a coarse-to-fine iterative cross-correlation algorithm (PIVview v.4.0, PIVTEC GmbH). The final interrogation sample size was set to $32 \times 6\,$pixel corresponding to a physical size of $\delta_x = 300\,\mu$m and $\delta_y = 55\,\mu$m. Table 1 presents these quantities in non-dimensional form. The combination of high spatial and temporal resolutions alongside the longer acquisitions allowed to resolve and analyze the flow spectra and statistics with great accuracy and detail.

RESULTS AND DISCUSSION

The performed plasma forcing shows to significantly affect the canonical wall normal profiles of the measurement-

Flow			PIV				PA					
Re_τ	u_τ	U_{cl}	f_s	$\frac{N_s U_{cl}}{f_s D/2}$	δ_x^+	δ_y^+	V_{pp}	L_x^+	λ_x^+	λ_z^+	$\min(V_{PA}^+)$	$\max(V_{PA}^+)$
	[m/s]	[m/s]	[kHz]				[kV]	$(\approx L_z^+)$		$(\equiv a^+)$		
8 000	0.27	7.51	0.8	2086	5.50	1.01	8	1150	570	110	-0.56	0.71
8 000	0.27	7.51	30	–	5.50	1.01	8	1150	570	110	-0.56	0.71
14 400	0.50	14.80	1.6	2055	10	1.83	8	2100	1050	200	-0.30	0.38
14 400	0.50	14.80	60	–	10	1.83	8	2100	1050	200	-0.30	0.38
14 400	0.50	14.80	1.6	2055	10	1.83	10	2100	1050	200	-0.30	0.46

Table 1. Main flow (Flow), flow diagnostics (PIV) and flow control (PA) parameters for the tested cases; quantities with the + superscript are made non-dimensional with the related flow-case inner scales.

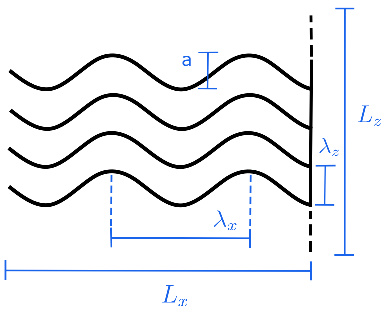

Figure 2. Schematics of the PA exposed electrodes and relevant geometric parameters as seen in Figure 1: flow coming from left to right.

accessible quantities: the velocity components along the streamwise (U for the time-averaged and u for the fluctuating terms) and wall normal (V and v) directions as well as the measured components of the Reynolds' stresses tensor ($\langle u_i u_j \rangle$, with $i, j \in [1\ 2]$). The mentioned profiles are shown in the left column of Figure 3 for the $Re_\tau = 8\,000$ unforced flow and in the right column for the plasma-forced flow at similar bulk flow conditions and at an input voltage of $V_{pp} = 8$ kV. All the profiles are normalized with the flow inner layer scales of the unforced flow. In particular, the friction velocity u_τ is measured from the global pipe static pressure measurements (see (Zanoun *et al.*, 2025)).

For the unforced flow, the agreement with the profiles of Pirozzoli (2024) obtained with DNS at $Re_\tau = 12\,000$ is very convincing with only the wall-normal velocity showing some non-zero, but very small – note that the plotted values are multiplied by 10 –, values close to the wall. In that region, despite the performed pre-processing, some measurement noise due to wall reflections and wobbling inevitably influences the presented data. The profile of the streamwise variance $\langle uu \rangle$ shows some deviations from the reference numerical data for $y^+ > 70$, featuring lower values. Nevertheless, this is to be expected given the experiments' lower Reynolds number. A further slight difference between the experimental and numerical data is shown from $y^+ \geq 10$ in all reported quantities, but overall the comparison can be deemed very satisfying considering the measurement challenges at the chosen Reynolds number. Furthermore, the measurements confirm that the actuator surface, when turned off, has no significant effects with respect to smooth-wall conditions.

When the PA array is operated at $V_{pp} = 8$ kV, all the reported statistic data appear much modified. The U profile features a dip in the range $10 \leq y^+ \leq 150$, where also the V component appears slightly enhanced, although, as commented, this quantity is more affected by measurement noise. Moving to the Reynolds stress terms, the performed forcing appears to considerably reduce the inner peak of $\langle uu \rangle$ whereas this term is much enhanced in the $30 \leq y^+ \leq 150$ region. At the same time, also the $\langle vv \rangle$ and $-\langle uv \rangle$ are augmented by the plasma jets. The larger $-\langle uv \rangle$ values for the controlled flow is evidence of a stronger wall-normal displacement of streamwise momentum from the control jets. The considered actuator in fact introduces regions of up-wash – where the wall-parallel jets over the encapsulated electrodes collide and lift off the wall – and down-wash – where, around the encapsulated electrodes, air is supplied to the control jets from the surrounding fluid. Moreover, these up- and down-wash regions are displaced along the pipe azimuthal direction as a result of the sinusoidal modulation of the exposed electrodes. Since we measured at only one azimuthal position of the PA array, these up- and down-motions cannot be separately inspected. Nevertheless, being the measurement plane downstream of the actuated region, the measured air particles have undergone both up- and down-wash motions. Consequently, the presented data are somewhat insensitive to the relative positioning of the actuator and laser sheet. Overall, it seems that the effect of the performed forcing is to shelter the wall region from turbulent events, while the increased shears from the induced jets enhance the flow fluctuations in the buffer and early logarithmic layers.

The spectral content of the three measured velocity fluctuations (*uu*, *vv* and *uv*) across the sampled wall-normal domain can be directly analyzed from the performed high-frequency measurements. The power spectral density (PSD) distributions of the three quantities are shown in the top and bottom row of Figure 4 for the unforced and the plasma-conditioned flows, respectively. The plasma forcing effectively reduces the kernel of larger *uu* PSD in the buffer and early logarithmic layers. These fluctuations feature a frequency content within the $0.01 \leq f^+ \leq 100$ band peculiar of the turbulence near wall structures, thus showing that the considered actuator has the authority of weakening their correlation. On the contrary, inspection of both the *vv* and *uv* PSD distributions evidences an opposite effect, with the plasma controlled flow showing larger PSD values in the $30 \leq y^+ \leq 100$ region. The shown PSD distributions corroborate the statistical Reynolds stresses profiles previously commented upon.

We consider now the larger Reynolds number flow ($Re_\tau = 14\,400$) where plasma jets of different intensities are deployed ($V_{pp} = [8, 10]$ kV). This was done to compensate for the expected reduced authority – in terms of V_{PA}^+ (see Table 1) – of

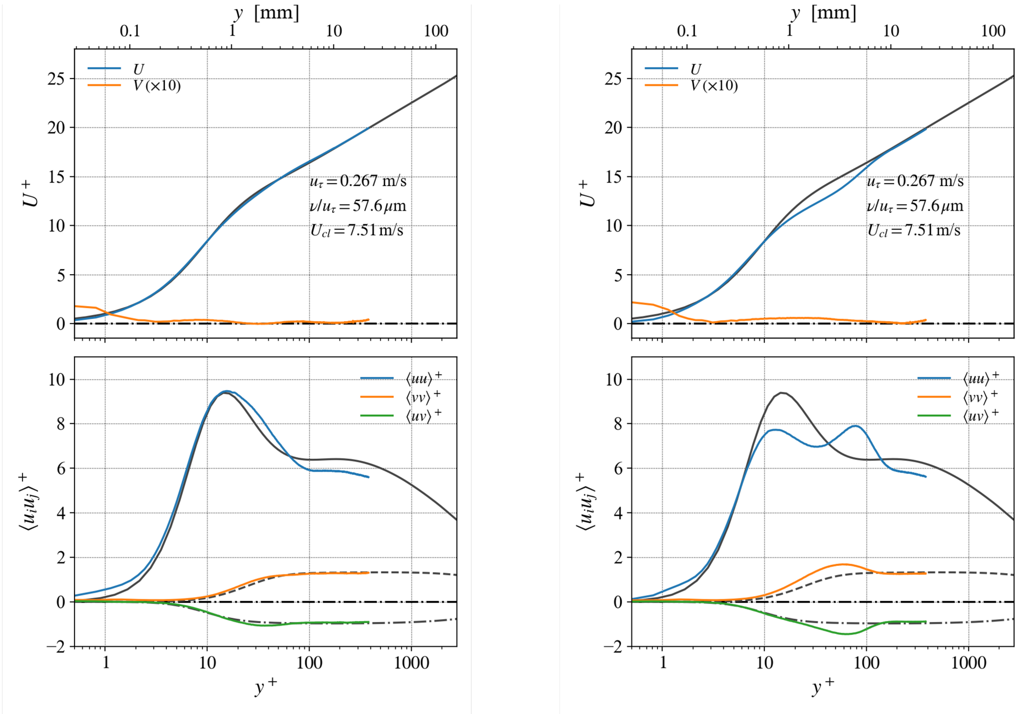

Figure 3. Time-averaged wall normal velocity profiles (top row) and Reynolds stresses profiles (bottom row) for the unforced flow (left column) and for the $V_{pp} = 8$ kV forced flow (right column) at $\mathrm{Re}_\tau = 8000$; the gray curves are from the DNS at $\mathrm{Re}_\tau = 12000$ by Pirozzoli (2024). The reported friction velocity (u_τ) was measured from the global pipe pressure drop, while the centerline velocity (U_{cl}) with a Prandtl tube.

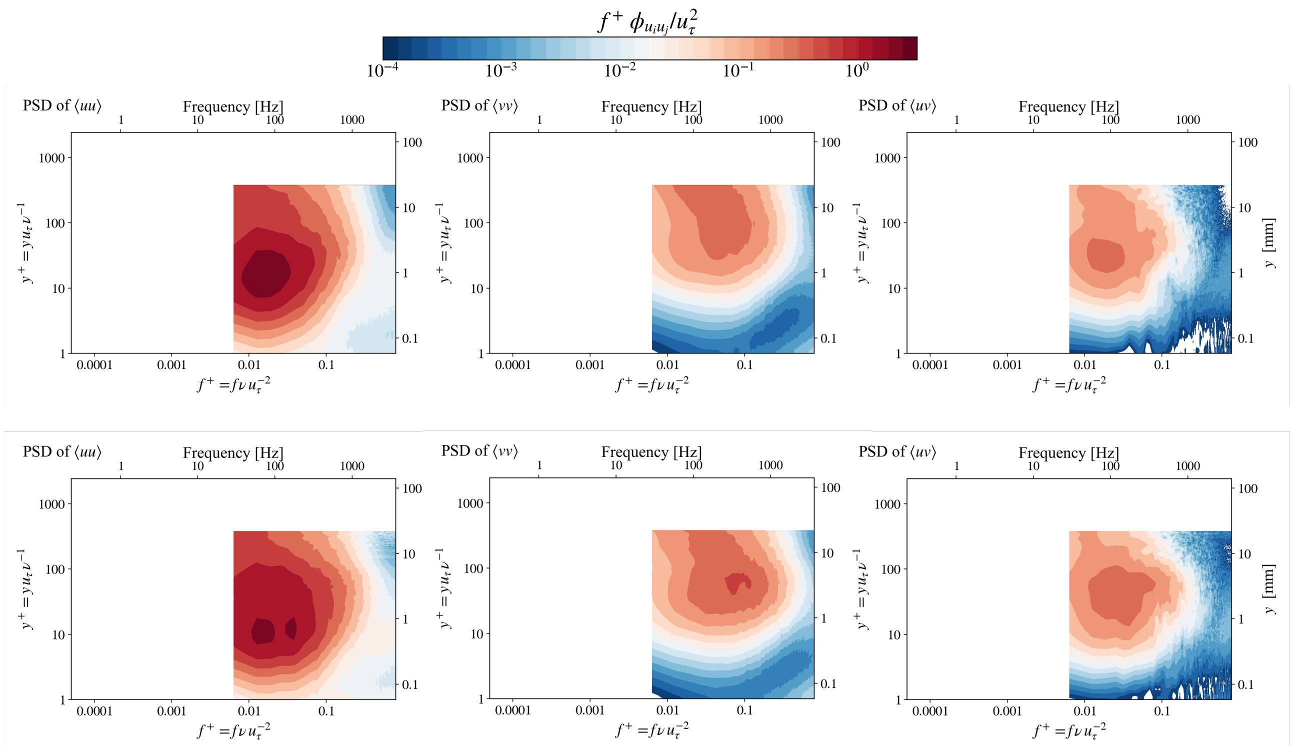

Figure 4. High-frequency *uu* (left column), *vv* (center column) and *uv* (right column) PSD distributions for the unforced flow (top row) and for the $V_{pp} = 8$ kV forced flow (bottom row) at $\mathrm{Re}_\tau = 8000$.

the considered flow actuator on the larger Reynolds number flow. The statistics wall-normal profiles for the uncontrolled flow well agree with the reference numerical data which are not shown for conciseness; whereas those for the $V_{pp} = 8$ (10) kV forced flow are reported in the left (right) column of Figure 5 (respectively). Starting from the time-averaged streamwise velocity profiles, it can be seen that the weaker-forcing flow features a small dip in the range $10 \leq y^+ \leq 150$ – as previously observed for the forced flow at lower Reynolds number –. This dip is more pronounced for the stronger-forcing flow. Again the V profiles show some non-zero values close to the wall due to measurement errors. Instead it appears that this quantity is slightly enhanced in the buffer and early logarithmic layers for the $V_{pp} = 10\,\text{kV}$ case. Considering now the measured Reynolds stresses terms, the forcing shows similar effects to those already reported for the $Re_\tau = 8\,000$ flow. Namely, the $\langle uu \rangle$ inner peak is reduced by the plasma jets, whereas the outer peak is enhanced. Also the $\langle vv \rangle$ and $-\langle uv \rangle$ peaks are augmented for the controlled cases. For all the mentioned quantities, the higher supplied voltage leads to stronger effects. These cases show that the considered actuator effectively conditions also the higher Reynolds number flow. Moreover, tuning the supplied voltage allowed to compensate for the larger friction velocity and the related smaller non-dimensional induced velocity (V_{PA}^+).

The wall-normal PSD distributions for the three measured correlated velocity components are shown in Figure 6 for the reference unforced flow (top row) and for the $V_{pp} = 8\,\text{kV}$ (bottom row) flows – the $V_{pp} = 10\,\text{kV}$ flow was measured only at the lower sampling frequency thus no high-frequency spectra for that case are available. For this higher Reynolds number, the effect of performed flow control is similar to what discussed for the $Re_\tau = 8\,000$ case. The induced jets reduce the correlation of the inner peak streamwise velocity fluctuations. The effect on the vv and uv spectra is instead milder for this case and mainly consists of enhanced PSD values further away from the wall.

CONCLUDING REMARKS

This study discusses the attempts done to actively condition the wall turbulence mechanisms at large Reynolds numbers. To do so, an unprecedented approach is followed: an array of sinusoidally-shaped DBD plasma actuators is installed in the Long Pipe facility of the CICLoPE laboratory. The pipe facility was operated at friction Reynolds numbers of $Re_\tau = 8\,000$ and $14\,400$. Advanced laser velocimetry was deployed just downstream of the controlled flow featuring very high spatial and temporal resolutions to deliver accurate flow statistics and spectral analyses.

The considered control successfully influenced the near wall flow-field with hindering the inner peak of the streamwise fluctuations while increasing the outer one. Similarly, the wall normal and the correlated streamwise wall-normal fluctuations resulted influenced by the plasma wall jets. The deployed control showed good authority at both the tested flow velocities as just increasing the supplied voltage amplitude, stronger control jets could be attained, thus compensating for the higher friction velocity. The presented study paves the way to active flow control efforts of turbulent flows of aeronautical interest aimed at controlling wall turbulence and friction drag.

ACKNOWLEDGMENTS

This study was carried out within the ”WAll-Turbulence Active COntrol” project – funded by European Union – Next Generation EU within the PRIN 2022 PNRR program (D.D.1409 del 14/09/2022 Ministero dell'Università e della Ricerca) and within the MOST – Sustainable Mobility National Research Center and received funding from the European Union Next-GenerationEU [PIANO NAZIONALE DI RIPRESA E RESILIENZA (PNRR) – MISSIONE 4 COMPONENTE 2, INVESTIMENTO 1.4 – D.D.1033 17/06/2022, CN00000023]. This manuscript reflects only the authors' views and opinions and the Ministry cannot be considered responsible for them.

REFERENCES

Bechert, D. W. & Bartenwerfer, M. 1989 *Journal of Fluid Mechanics* **206**, 105–129.

Bellani, G. & Talamelli, A. 2016 *Springer Proceedings in Physics* pp. 205–209.

Benard, N., Moreau, E. & Bonnet, J. P. 2024 Drag reduction by wall-parallel standing wave with plasma actuator. In *AIAA SciTech Forum and Exposition, 2024*. AIAA.

Cafiero, G., Amico, E. & Iuso, G. 2024 *Journal of Fluid Mechanics* **984**, A59.

Choi, K.-S. & Graham, M. 1998 *Physics of Fluids* **10**, 7–9.

Choi, K.-S., Jukes, T. & Whalley, R. 2011 *Philosophical Transactions of the Royal Society A: Mathematical, Physical and Engineering Sciences* **369**, 1443–1458.

Fang, Z., Zong, H., Zhang, X., Wu, Y., Su, Z., Liang, H. & Bian, D. 2024 *Physics of Fluids* **36**.

Hehner, M. T., Gatti, D. & Kriegseis, J. 2019 *Physics of Fluids* **31**, 1–6.

Iuso, G., Onorato, M., Spazzini, P. G. & Cicca, G. M. Di 2002 *Journal of Fluid Mechanics* .

Jukes, T. N., Choi, K.-S., Johnson, G. A. & Scott, S. J. 2006 *Collection of Technical Papers - 3rd AIAA Flow Control Conference* **3**, 1687–1700.

Jung, W. J., Mangiavacchi, N. & Akhavan, R. 1992 *Physics of Fluids A* **4**, 1605–1607.

Peet, Y. & Sagaut, P. 2009 *Physics of Fluids* **21**, 105105.

Pirozzoli, S. 2024 *Journal of Fluid Mechanics* **989**, A5.

Sasamori, M., Iihama, O., Mamori, H., Iwamoto, K. & Murata, A. 2017 *Flow, Turbulence and Combustion 2017 99:1* **99**, 47–69.

Sasamori, M., Mamori, H. & Iwamoto, K. 2014 *Experiments in Fluids 2014 55:10* **55**, 1828–.

Schoppa, W. & Hussain, F. 1998 *Physics of Fluids* **10**, 1049–1051.

Serpieri, J., Hehner, M. T. & Kriegseis, J. 2023 *Flow, Turbulence and Combustion* pp. 1–17.

Thomas, F. O., Corke, T. C., Duong, A., Midya, S. & Yates, K. 2019 *Journal of Physics D: Applied Physics* **52**.

Walsh, M. J. 2012 *https://doi.org/10.2514/3.60126* **21**, 485–486.

Wei, X. & Zhou, Y. 2025 *Journal of Fluid Mechanics* **1007**, R5.

Whalley, R. D. & Choi, K.-S. 2014 *Experiments in Fluids* **55**.

Wilkinson, S. P. 2003 *41st Aerospace Sciences Meeting and Exhibit* .

Willert, C. E., Soria, J., Stanislas, M., Klinner, J., Amili, O., Eisfelder, M., Cuvier, C., Bellani, G., Fiorini, T. & Talamelli, A. 2017 *Journal of Fluid Mechanics* **826**, R5.

Zanoun, E.-S., Bauer, C., Wagner, C., Durst, F., Egbers, C., Bellani, G. & Talamelli, A. 2025 *Journal of Turbulence* **26** (8-9), 251–272.

Zheng, X., Bellani, G., Mascotelli, L., Örlü, R., Ianiro, A., Vila Sanmiguel, C., Discetti, S., Serpieri, J., Raiola, M., Talamelli, A., Li, Y. & Jiang, N. 2022 *Experimental Thermal and Fluid Science* **131**, 110529.

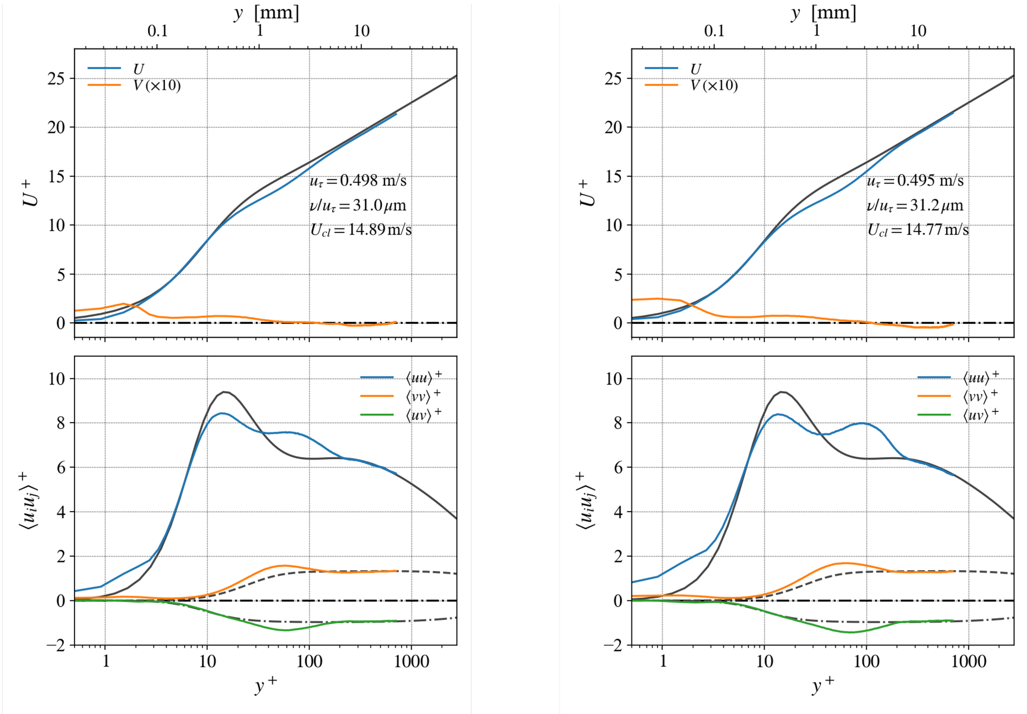

Figure 5. Time-averaged wall normal velocity profiles (top row) and Reynolds stresses profiles (bottom row) for the $V_{pp} = 8\,$kV forced flow (left column) and for the $V_{pp} = 10\,$kV forced flow (right column) at $\mathrm{Re}_\tau = 14400$; the gray curves are from the DNS at $\mathrm{Re}_\tau = 12000$ by Pirozzoli (2024). The reported friction velocity (u_τ) was measured from the global pipe pressure drop, while the centerline velocity (U_{cl}) with a Prandtl tube.

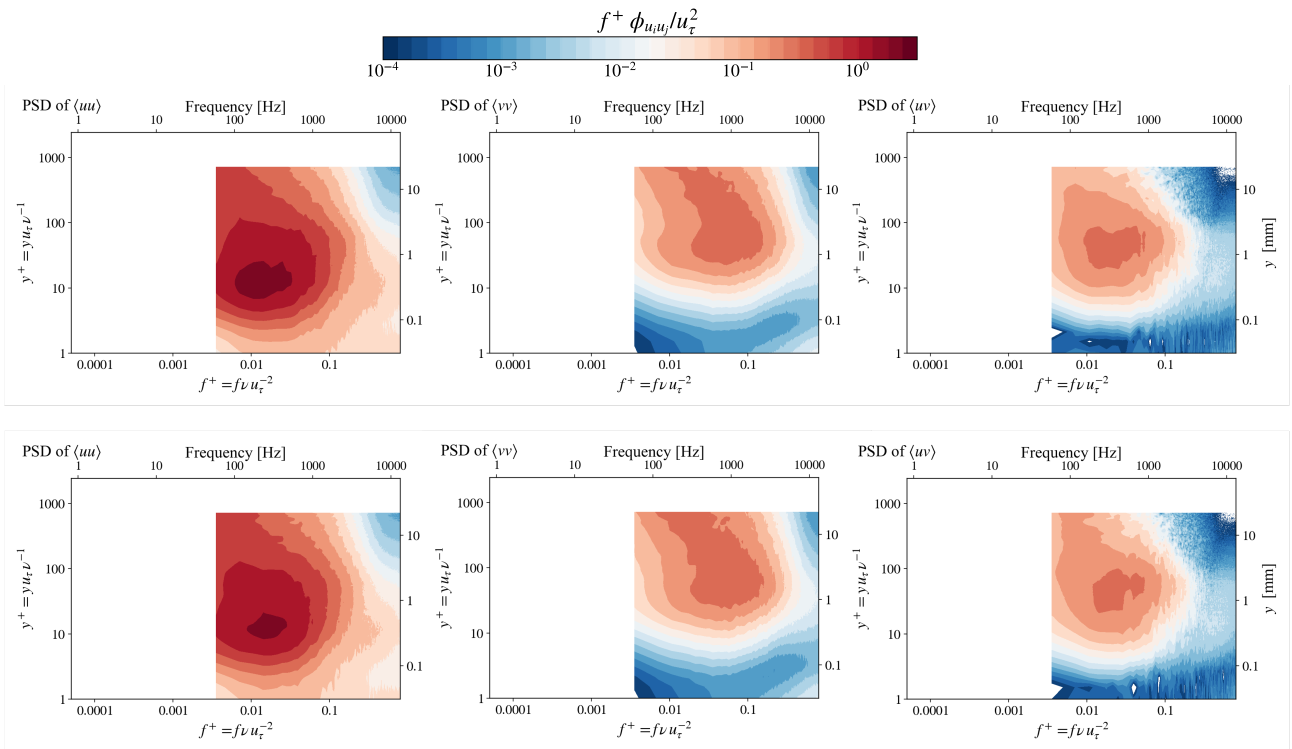

Figure 6. High-frequency uu (left column), vv (center column) and uv (right column) PSD distributions for the unforced flow (top row) and for the $V_{pp} = 8\,$kV forced flow (bottom row) at $\mathrm{Re}_\tau = 14400$.